

Article

Apatite-Forming Ability and Visible Light-Enhanced Antibacterial Activity of CuO-Supported TiO₂ Formed on Titanium by Chemical and Thermal Treatments

Po-Cheng Sung¹, Taishi Yokoi² , Masaya Shimabukuro² , Takayuki Mokudai^{3,4} and Masakazu Kawashita^{2,*} 

- ¹ Graduate School of Medical and Dental Sciences, Tokyo Medical and Dental University, Bunkyo-ku, Tokyo 113-8549, Japan; foster01506@gmail.com
- ² Institute of Biomaterials and Bioengineering, Tokyo Medical and Dental University, 2-3-10 Kanda-Surugadai, Chiyoda-ku, Tokyo 101-0062, Japan; yokoi.taishi.bcr@tmd.ac.jp (T.Y.); shimabukuro.bcr@tmd.ac.jp (M.S.)
- ³ Joining and Welding Research Institute, Osaka University, 11-1 Mihogaoka, Ibaraki, Osaka 567-0047, Japan; tmokudai.jwri@osaka-u.ac.jp or tmokudai@tohoku.ac.jp
- ⁴ Institute of Materials Research, Tohoku University, 2-1-1 Katahira, Aoba-ku, Sendai, Miyagi 980-8577, Japan
- * Correspondence: kawashita.bcr@tmd.ac.jp

Abstract: Titanium with apatite-forming ability as well as antibacterial activity is useful as a component of antibacterial dental implants. When Ti was subjected to hydrogen peroxide (H₂O₂), copper acetate (Cu(OAc)₂), and heat (H₂O₂-Cu(OAc)₂-heat) treatments, a network structure of anatase and rutile titanium dioxide (TiO₂) and fine copper oxide (CuO) particles was formed on the Ti surface. The resulting samples accumulated a dense and uniform apatite layer on the surface when incubated in simulated body fluid and showed enhanced antibacterial activity against *Escherichia coli* and *Staphylococcus aureus* under visible-light irradiation. Electron spin resonance spectra of H₂O₂-Cu(OAc)₂-heat-treated samples showed that hydroxyl radicals (\cdot OH) were generated from the samples, and the concentration of \cdot OH increased with increasing Cu concentration of the Cu(OAc)₂ solution. The enhanced antibacterial activity of these samples under visible-light irradiation may be attributable to the generation of \cdot OH from samples. These results suggest that Ti implants obtained using H₂O₂-Cu(OAc)₂-heat treatments and subjected to regular or on-demand visible-light irradiation may provide a decreased risk of peri-implantitis.

Keywords: titanium; CuO; TiO₂; apatite; antibacterial activity; photocatalytic activity



Citation: Sung, P.-C.; Yokoi, T.; Shimabukuro, M.; Mokudai, T.; Kawashita, M. Apatite-Forming Ability and Visible Light-Enhanced Antibacterial Activity of CuO-Supported TiO₂ Formed on Titanium by Chemical and Thermal Treatments. *J. Funct. Biomater.* **2024**, *15*, 114. <https://doi.org/10.3390/jfb15050114>

Academic Editor: Christie Ying Kei Lung

Received: 19 March 2024
Revised: 19 April 2024
Accepted: 21 April 2024
Published: 24 April 2024



Copyright: © 2024 by the authors. Licensee MDPI, Basel, Switzerland. This article is an open access article distributed under the terms and conditions of the Creative Commons Attribution (CC BY) license (<https://creativecommons.org/licenses/by/4.0/>).

1. Introduction

With increases in the number of dental implants installed, peri-implant diseases have become more common. Such diseases can be broadly classified into peri-implant mucositis and peri-implantitis. Peri-implant mucositis, considered a precursor to peri-implantitis, is defined as a reversible inflammation that is localized to the surrounding mucosal tissue and does not involve bone resorption. On the other hand, peri-implantitis is defined as an irreversible inflammation that involves soft tissue inflammation and bone resorption around the implant [1]; prolonged peri-implantitis leads to implant failure. As assessed at greater than 5 years after dental implant placement, the prevalence of peri-implantitis is estimated to be 10% to 37% at the patient level and 7% to 27% at the implant level [2–7]. Classically, surgical treatment has been the main therapy for peri-implantitis; however, in recent years, chemotherapy using antibiotics and anti-inflammatory drugs has been employed to treat invasive and severe peri-implantitis [8,9]. However, surgical treatment is itself highly invasive, and there are concerns about the emergence of drug-resistant bacteria due to the use of antibiotics and anti-inflammatory drugs [10].

In recent years, there has been ongoing development of antimicrobial therapies using micromaterials and nanomaterials. Titanium-based metal organic frameworks (Ti-MOFs)

have been investigated for use in therapeutic areas, including the treatment of bacterial infection, cancer, inflammation, and bone injury [11]; notably, MOF-loaded biohybrid magnetic microrobots have been shown to achieve good dispersion and targeted mobility with enhanced antibacterial efficiency [12]. Surface-modified nanomaterials also have been proposed to achieve passive or active targeted antibacterial effects [13,14]. Furthermore, materials that possess topographical features with high aspect ratios show bactericidal activity [15,16]. However, it remains unclear whether any of these materials are effective in treating peri-implantitis. The use of titanium dental implants with antibacterial activity as well as osteoconductivity has been shown to reduce the risk of peri-implantitis. To date, many surface treatments of Ti have been proposed to impart antibacterial activity as well as osteoconductivity to this metal [17–25]. Orthopedic implants coated with silver-containing hydroxyapatite [26] are employed clinically in Japan, but dental implants with both antibacterial activity and osteoconductivity are not yet in clinical use. If TiO₂ with visible-light-responsive photocatalytic antibacterial activity were generated on the abutment of Ti dental implants, the risk of peri-implantitis might be reduced by regular or on-demand visible-light exposure in the dental clinic. One candidate for the visible light source is a light-emitting diode (LED) light used in teeth whitening, but this LED light has been shown to exhibit difficulty in penetrating the gingiva and reaching the abutment of the dental implants. Therefore, the visible light-responsive antibacterial activity of the dental implants would be expected to be enhanced when the abutment is not completely covered by periodontal tissue. In previous work, our laboratory has attempted to generate copper-doped titanium dioxide (TiO₂) on Ti by chemical and thermal treatments [27,28]. This approach acknowledges that TiO₂ generated by such strategies has been shown to bond to living bone [29] and that Cu-doped TiO₂ demonstrates visible-light-induced photocatalytic antibacterial activity [30–32]. Some metals other than Cu, such as silver and zinc, also exhibit antibacterial effects, but the visible-light-induced antibacterial effects cannot be expected for Ag- or Zn-doped TiO₂. In this context, we reported that Cu-doped TiO₂ formed on Ti when Ti was subjected to (sequentially) immersion in a sodium hydroxide solution, immersion in a Cu-containing aqueous solution, and heating at 600 °C for 1 h. Apatite was observed to accumulate on the surface of the resulting Ti within 7 days of incubation in simulated body fluid (SBF) [27,28], and the resulting sample exhibited antibacterial activity against *Escherichia coli* under visible-light irradiation [28]. However, the apatite formed only on a part of the sample surface, indicating that the sample had limited apatite-forming ability. Furthermore, the antibacterial activity of the sample was not assessed against Gram-positive bacteria such as *Staphylococcus aureus*.

In the present study, we induced the formation of Cu-doped TiO₂ on Ti by subjecting the Ti to (sequentially) immersion in a hydrogen peroxide solution, immersion in a copper acetate (Cu(OAc)₂) solution, and thermal treatment. Previous work showed that a TiO₂ layer is formed on Ti by sequential treatment with an aqueous NaOH solution, hot water, and heat [29,33], but surface treatments involving immersion in a H₂O₂ solution also are known to generate a TiO₂ layer on Ti [34–38]. In that previous work, we found that the TiO₂ layer (which forms on Ti following such treatment) accumulates apatite when the sample is incubated in SBF [34,36–38]; this apatite permits bonding to living bone [35]. Therefore, from the perspective of simplifying surface treatment, treatment with H₂O₂ solution was employed to induce the formation of a TiO₂ layer on Ti in the present study. Furthermore, we used a Cu(OAc)₂ solution for Cu doping into TiO₂, a strategy that suppresses the undesired dissolution of the TiO₂ layer that otherwise results from immersion in acidic Cu-containing solutions such as copper nitrate (Cu(NO₃)₂) [27]. We additionally evaluated the resulting samples for surface structure, apatite-forming ability, and Cu release. Furthermore, we investigated the generation by the samples of hydroxyl radicals (\cdot OH), a reactive oxygen species (ROS), and assessed the antibacterial activity of samples against *S. aureus* as well as *E. coli*, both with and without visible-light irradiation.

2. Materials and Methods

2.1. Sample Preparation

Commercially pure Ti (99.5%) (Test Materials Co., Ltd., Tokyo, Japan) was employed in this study. The Ti was provided in the form of 8-mm diameter cylindrical rods, which subsequently were sliced into 1.0-mm thick sections. Following slicing, the surfaces of the disks were subjected to mechanical polishing using a diamond pad (No. 400; Maruto Instrument Co., Ltd., Tokyo, Japan). The polished Ti disks were washed ultrasonically, for 10 min per cycle, once with acetone (99%; Nacalai Tesque, Inc., Kyoto, Japan) and then twice with ultrapure water. The washed Ti disks were then dried at room temperature and atmospheric pressure. Each dried Ti disk was immersed in 10 mL of a 30 vol% H₂O₂ aqueous solution (FUJIFILM Wako Pure Chemical Corp., Osaka, Japan) in an ECK-50ML-R polypropylene tube (AS-ONE Corp., Osaka, Japan), and the tube then was heated at 80 °C for 1 h using a BW101 water bath (Yamato Scientific Co., Ltd., Tokyo, Japan). The samples were removed from the H₂O₂ aqueous solution and immersed in Cu(OAc)₂ aqueous solutions at various concentrations (1, 10, or 100 mM) in a polypropylene tube at 80 °C for 24 h using the water bath. After the Cu(OAc)₂ treatment, the disk was removed from the solution, washed with ultrapure water, and then dried at room temperature and atmospheric pressure. Each Ti disk that had been treated sequentially with the H₂O₂ and Cu(OAc)₂ solutions was then heat-treated at 600 °C for 1 h using an FO101 electric furnace (Yamato Scientific Co., Ltd.). Surface treatments and the sample designations are listed in Table 1.

Table 1. Surface treatments and names of samples.

Surface Treatment	Sample Name
None	TI
H ₂ O ₂ + heat	HP
H ₂ O ₂ + 1 mM Cu(OAc) ₂ + heat	Cu1
H ₂ O ₂ + 10 mM Cu(OAc) ₂ + heat	Cu10
H ₂ O ₂ + 100 mM Cu(OAc) ₂ + heat	Cu100

2.2. Surface Analysis of Samples

Many of the experimental protocols and conditions described in Sections 2.2–2.6 are essentially identical to those used in previous studies [28,39]. The surface morphology of each sample was observed using a JSM-7900F field emission scanning electron microscope (FE-SEM; JEOL, Tokyo, Japan). A mapping image of the sample was obtained using a JED-2300 energy dispersive X-ray spectrometer (JEOL) attached to the FE-SEM. The crystalline phase of the sample surface layer was identified using a MiniFlex600 X-ray diffractometer (XRD; Rigaku Corporation, Tokyo, Japan) with Cu K α radiation.

The composition of the surface layer was evaluated using a JPS-9010MC X-ray photoelectron spectroscopy (XPS) instrument (JEOL). Monochromatic Mg K α radiation (1253.6 eV) at 10 kV and 10 mA was used as the X-ray source. The C 1s photoelectron peak at 285.0 eV was used as a reference to calibrate the binding energy. The XPS peak was analyzed using CasaXPS (version 2.3.24; Casa Software, Ltd., Devon, UK). The chemical state of Cu on the samples was determined using a modified Auger parameter, which was calculated as described previously [22]. We conducted background subtraction using the CasaXPS software, following Shirley's method [40] to calculate the integrated intensity of peaks. The surface composition of the samples was calculated using CasaXPS while employing the following relative sensitivity factors: C 1s (1.00), O 1s (2.93), P 2p (1.192), Ca 2p (5.07), Ti 2p (7.81), and Cu 2p_{3/2} (16.73). The proportions of (Cu⁰ + Cu⁺) and Cu²⁺ at the sample surface were calculated using the following equations [41]:

$$\% (\text{Cu}^0 + \text{Cu}^+) = (A - (A_{1s}/B_s) \times B)/(A + B) \times 100 \quad (1)$$

$$\% (\text{Cu}^{2+}) = B (1 + (A_{1s}/B_s))/(A + B) \times 100 \quad (2)$$

where A is the total area of the Cu $2p_{3/2}$ peak, B is the area of the shake-up peak, and A_{1s}/B_s is the ratio of the Cu $2p_{3/2}$ peak/shake-up peak areas. In the present study, the A_{1s}/B_s ratio was fixed at the value of 1.89 expected for CuO.

2.3. Evaluation of In Vitro Apatite-Forming Ability of Sample

The apatite-forming ability of the samples was evaluated using an SBF [42,43] that contained ions at concentrations (Na^+ , 142.0 mM; K^+ , 5.0 mM; Ca^{2+} , 2.5 mM; Mg^{2+} , 1.5 mM; Cl^- , 147.8 mM; HCO_3^- , 4.2 mM; HPO_4^{2-} : 1.0 mM; SO_4^{2-} , 0.5 mM) nearly identical to those found in human blood plasma. We prepared the SBF according to the ISO 23317:2014 [43] protocol. All chemicals used for SBF formulation were purchased from Nacalai Tesque, Inc. (Kyoto, Japan). A volume of 30 mL of the prepared SBF was dispensed into an ECK-50ML-R centrifuge tube. The samples were immersed in the SBF at 36.5 °C for 7 days. The samples were then removed from the SBF, gently rinsed with ultrapure water, and dried at approximately 25 °C and atmospheric pressure. The lower surface of each sample was observed using a VE8800 scanning electron microscope (SEM; Keyence Corp., Osaka, Japan) and XRD.

2.4. Measurement of Cu Ion-Release Behavior of Sample

To investigate the Cu ion-release behavior of each sample, an aliquot (10 mL) of phosphate-buffered saline (PBS; Catalog 166-23555; FUJIFILM Wako Pure Chemical Corp., Osaka, Japan) was dispensed into an ECK-50ML-R centrifuge tube. The sample ($n = 3$) was immersed in PBS and the tube was maintained at 36.5 °C. The PBS was refreshed at appropriate periods. The amounts of Cu ions (per time point and cumulative) released from the samples were calculated at 1, 3, 7, 14, and 28 days based on the Cu concentrations in the PBS, which were measured using an ICP-7000 inductively coupled plasma atomic emission spectroscopy (ICP-AES) instrument (Shimadzu Corp., Kyoto, Japan). Figure 1 shows a schematic diagram of the Cu ion-release assay.

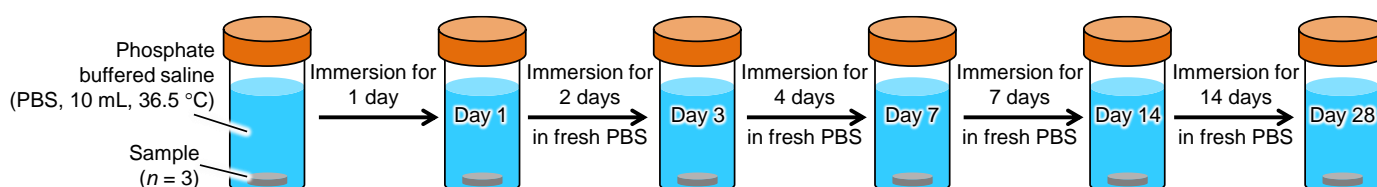


Figure 1. Schematic diagram of Cu ion-release assay. PBS, phosphate-buffered saline.

2.5. Evaluation of Antimicrobial Activity of Sample

The antibacterial activity of each sample was evaluated using strains of *S. aureus* (NBRC1221355; obtained from the NITE Biological Resource Center, Chiba, Japan) and *E. coli* (NBRC39725; also obtained from the NITE Biological Resource Center) according to the method described in JIS R 1752:2020 [44]. This experiment was approved by the Pathogenic Organisms Safety Management Committee of the Tokyo Medical and Dental University (Approval No. M22022-002; Approval date: 25 April 2022). *S. aureus* and *E. coli* were cultivated in soybean-casein digest (SCD) broth (Nissui Pharmaceutical Co., Ltd., Tokyo, Japan) or Luria–Bertani (LB) broth (MP Biomedicals, CA, USA), respectively, at 37 °C for 24 h. The resulting *S. aureus* cells were pelleted and resuspended in PBS at a density of 4.3×10^7 to 1.0×10^8 colony-forming units (CFU)/mL. Similarly, the resulting *E. coli* cells were pelleted and resuspended in PBS at a density of 3.2×10^7 to 1.0×10^8 CFU/mL. An antibacterial activity test was performed in quadruplicate ($n = 4$) for each sample, as described below.

Briefly, the sample (a Ti disc) was placed on a Falcon® bacteriological petri dish (Catalog No. 351029; Corning, Inc., Corning, NY, USA) with the sample surface facing upward; an aliquot (10 µL) of the test bacterial suspension then was dispensed onto the sample. Subsequently, the sample surface was covered with plastic film (Catalog No.

JPG533090; A.R. Medicom Inc. (Asia), Ltd., Kobe, Japan) to ensure close contact. The petri dish then was placed in a GB-2.0L gas barrier box (AS ONE Corp., Osaka, Japan). To reduce the effects on the bacteria of increasing temperature and drying during visible-light irradiation, pure water was dispensed into the bottom of the gas barrier box to maintain a relative humidity exceeding 90%. A 460-nm LED lamp (Model SPA-10SW; Hayashi Clock Industry Co., Ltd., Tokyo, Japan) was used as the light source. The distance from the lower part of the lens to the sample surface was 10 cm; the irradiance and the irradiation period were 250 W/m² and 30 min, respectively. These irradiation parameters were defined based on the distance that might be expected between a visible-light source and the abutment of dental implants during dental treatment in the clinic. Following the visible-light irradiation, bacteria adhering to the sample and plastic film were recovered by washing with 1 mL of PBS. The resulting test bacterial suspension was subjected to 10-fold serial dilution in PBS, and aliquots (100 µL) of the 10-fold and 100-fold dilutions were plated on SCD agar (*S. aureus*) or LB agar (*E. coli*). After incubation at 37 °C for 24 h, the number of bacterial colonies formed on the plate surface was counted. The number of viable bacteria was calculated using the following formula:

$$N = Z \times E \times 10 \quad (3)$$

where N , Z , and E are the viable bacterial count, arithmetic mean number of colonies, and dilution factor, respectively.

2.6. Measurement of ROS Generated by Samples

It is difficult to directly measure ROS and free radicals at room temperature (approximately 25 °C). Instead, we employed electron spin resonance (ESR) using a spin-trapping method to measure the ROS generated from samples irradiated with visible light. ESR was conducted using a JES-FA-100 instrument (JEOL, Ltd.). The spin-trapping agent consisted of 5,5-dimethyl-1-pyrroline-*N*-oxide (DMPO; Labotech Co., Tokyo, Japan). The ESR measurement was conducted under the following conditions: microwave power, 4.0 mW; microwave frequency, 9428.954 MHz; magnetic width, 0.1 mT; field sweep width, ±5 mT; field modulation frequency, 100 kHz; modulation width, 0.1 mT; time constant, 0.03 s; and sweep time, 0.1 min. Each sample was placed in a well of a 24-well plate, and 300 mM DMPO was dispensed at 500 µL/well. The samples immersed in the DMPO solution were irradiated with visible light, using the same 460-nm LED lamp for 30 min under the same conditions as those in the antibacterial property test. Subsequently, 200 µL of the DMPO solution (in which the sample had been immersed) was removed from each well and assessed for ROS using the ESR spectrometer. Hydroxyl radicals were quantified using 4-hydroxy-2,2,6,6-tetramethylpiperidine-1-oxyl (TEMPOL; Sigma-Aldrich, St. Louis, MO, USA) as the standard. The areas of DMPO-OH spectra were compared with that of a 2 µM TEMPOL standard measured under identical settings to estimate the concentration of the DMPO-OH adduct.

2.7. Statistical Analysis

Statistical analyses were performed using Microsoft Excel version 2209 (Microsoft, Redmond, WA, USA). One-way analysis of variance followed by multiple-hypothesis tests (Tukey's honestly significant difference tests) was performed for comparisons between more than two groups. $p < 0.01$ was considered statistically significant.

3. Results

XRD peaks attributable to anatase- and rutile-type TiO₂ were observed for all samples other than Sample TI; peaks attributable to copper oxide (CuO) were observed for samples Cu1, Cu10, and Cu100 (Figure 2). As the Cu(OAc)₂ concentration increased, the intensity ratio of the XRD peak of rutile-type TiO₂ around 27.7° in 2θ to that of anatase-type TiO₂ around 25.5° in 2θ also increased.

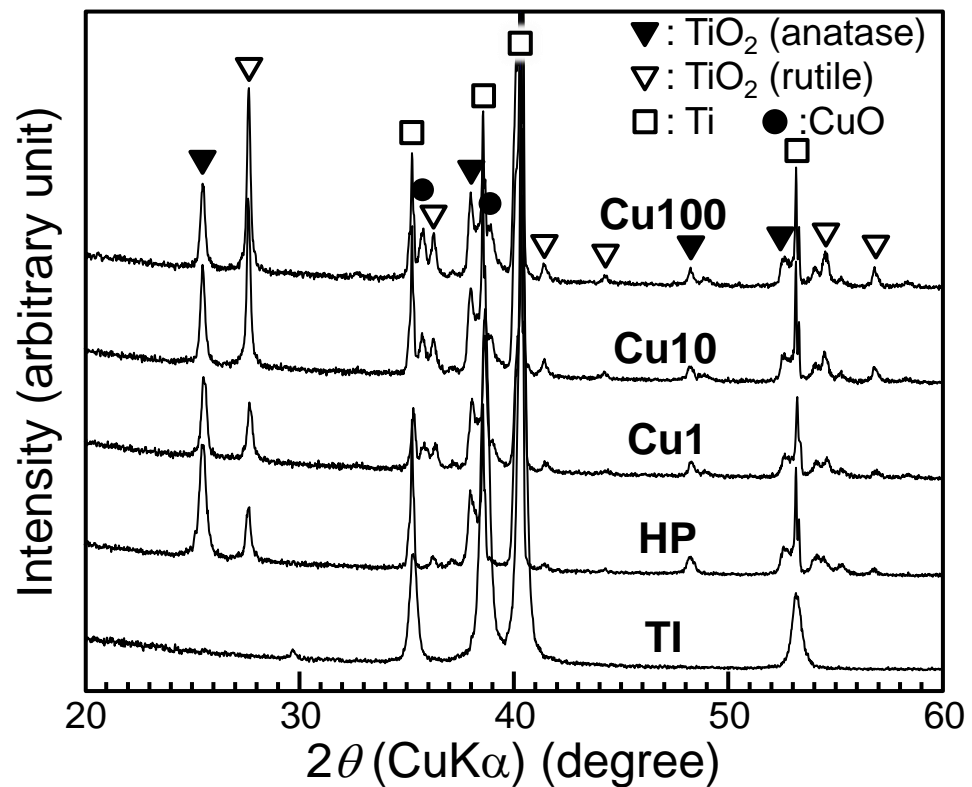


Figure 2. XRD patterns of samples. XRD: X-ray diffraction, TI: sample with no treatment, HP: sample with H_2O_2 treatment, Cu1: sample with H_2O_2 , 1 mM $\text{Cu}(\text{OAc})_2$, and heat treatment, Cu10: sample with H_2O_2 , 10 mM $\text{Cu}(\text{OAc})_2$, and heat treatment, Cu100: sample with H_2O_2 , 100 mM $\text{Cu}(\text{OAc})_2$, and heat treatment.

FE-SEM micrographs (Figure 3A) showed that a fine network structure formed on the surface of the HP, Cu1, Cu10, and Cu100 samples and that fine particles formed on the Cu1, Cu10, and Cu100 samples. At the macroscopic level, the HP sample exhibited a brown color, while the Cu1, Cu10, and Cu100 samples exhibited a black color (insets in Figure 3A). The EDS mapping images of the samples (Figure 3B) indicated that the fine particles that formed on the Cu1, Cu10, and Cu100 samples were composed primarily of Cu and O.

In the XPS spectra of the Cu1, Cu10, and Cu100 samples, XPS peaks located in the C 1s, Ti 2p, O 1s, and Cu 2p energy regions were detected on the surfaces of the samples. The binding energy of the Ti 2p_{3/2} peak for the Cu1, Cu10, and Cu100 samples was approximately 458.8 eV (Figure 4A), indicating that Ti existed primarily as TiO_2 in these samples [45,46]. The binding energies of the Cu 2p_{3/2} peaks for the Cu1, Cu10, and Cu100 samples were located at approximately 933.5, 933.7, and 933.7 eV, respectively (Figure 4B); the modified Auger parameters for the Cu1, Cu10, and Cu100 samples were measured at 1850.6, 1850.9, and 1850.7 eV, respectively. These results indicated that the Cu in these samples existed primarily as Cu^{2+} [22,41]. The concentrations of Cu on the surfaces of the Cu1, Cu10, and Cu100 samples were 6.8, 15.8, and 12.9 atomic%, respectively. For all three of these samples, the proportions of ($\text{Cu}^0 + \text{Cu}^+$) and Cu^{2+} ranged from 19.2 to 26.5% and 73.5–80.8%, respectively (Table 2).

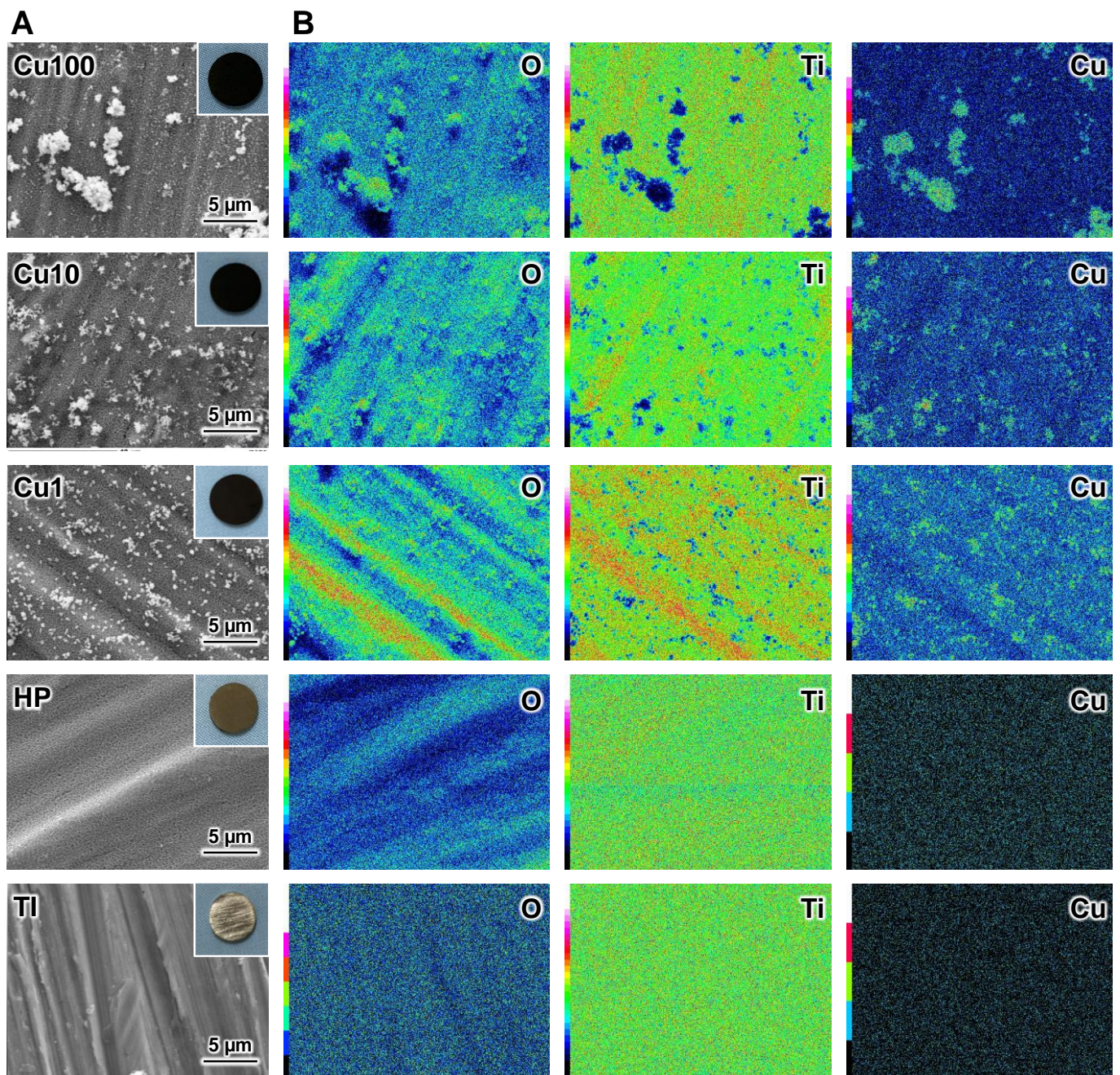


Figure 3. FE-SEM micrographs with insets showing macroscopic appearance (A), and EDS elemental mapping images (B) of samples. FE-SEM: field emission scanning electron microscope, EDS: energy dispersive X-ray spectrometer, TI: sample with no treatment, HP: sample with H_2O_2 treatment, Cu1: sample with H_2O_2 , 1 mM $Cu(OAc)_2$, and heat treatment, Cu10: sample with H_2O_2 , 10 mM $Cu(OAc)_2$, and heat treatment, Cu100: sample with H_2O_2 , 100 mM $Cu(OAc)_2$, and heat treatment. The color bar represents the intensity of EDS signal (black: low intensity, red or pink: high intensity).

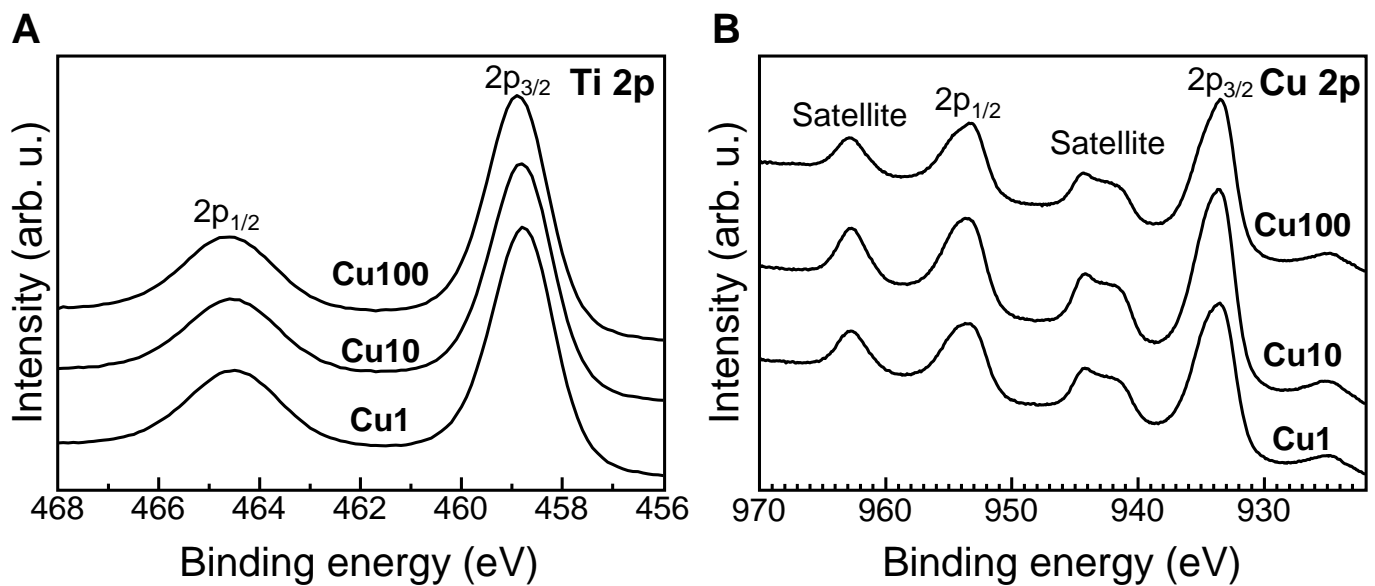


Figure 4. XPS narrow spectra in the Ti 2p (A) and Cu 2p (B) energy regions for the Cu1, Cu10, and Cu100 samples. XPS: X-ray photoelectron spectroscopy, arb. u.: arbitrary unit, Cu1: sample with H₂O₂, 1 mM Cu(OAc)₂, and heat treatment, Cu10: sample with H₂O₂, 10 mM Cu(OAc)₂, and heat treatment, Cu100: sample with H₂O₂, 100 mM Cu(OAc)₂, and heat treatment.

Table 2. Concentrations of Cu and proportions of Cu species at the surfaces of the Cu1, Cu10, and Cu100 samples. at.%: atomic percent, Cu1: sample with H₂O₂, 1 mM Cu(OAc)₂, and heat treatment, Cu10: sample with H₂O₂, 10 mM Cu(OAc)₂, and heat treatment, Cu100: sample with H₂O₂, 100 mM Cu(OAc)₂, and heat treatment.

Sample	Concentration of Cu (at.%)	Proportion of Cu Species (%)	
		Cu ⁰ + Cu ⁺	Cu ²⁺
Cu1	6.8	20.1	79.9
Cu10	15.8	19.2	80.8
Cu100	12.9	26.5	73.5

SEM photographs and XRD patterns of samples following 7 days of incubation in SBF are shown in Figure 5. The HP, Cu1, Cu10, and Cu100 samples accumulated dense and uniform layers after a week of immersion in SBF, and XRD peaks attributable to apatite were observed for these samples.

When samples were immersed in PBS for periods of up to 28 days, the concentration of Cu eluted from the samples increased gradually (Figure 6). However, no statistically significant differences were observed in the eluted Cu ion concentration when comparing the samples at a given immersion time point.

With or without visible-light irradiation, the viable counts of *S. aureus* and *E. coli* did not differ significantly when comparing between the HP and TI samples; in contrast, viable counts for both bacterial species were decreased significantly, with and without irradiation, in the Cu1, Cu10, and Cu100 samples (compared to the TI sample) (Figure 7). Notably, among samples irradiated with visible light, the viable counts of *E. coli* in the Cu1, Cu10, and Cu100 samples were decreased by more than two logs compared to similarly treated TI and HP samples.

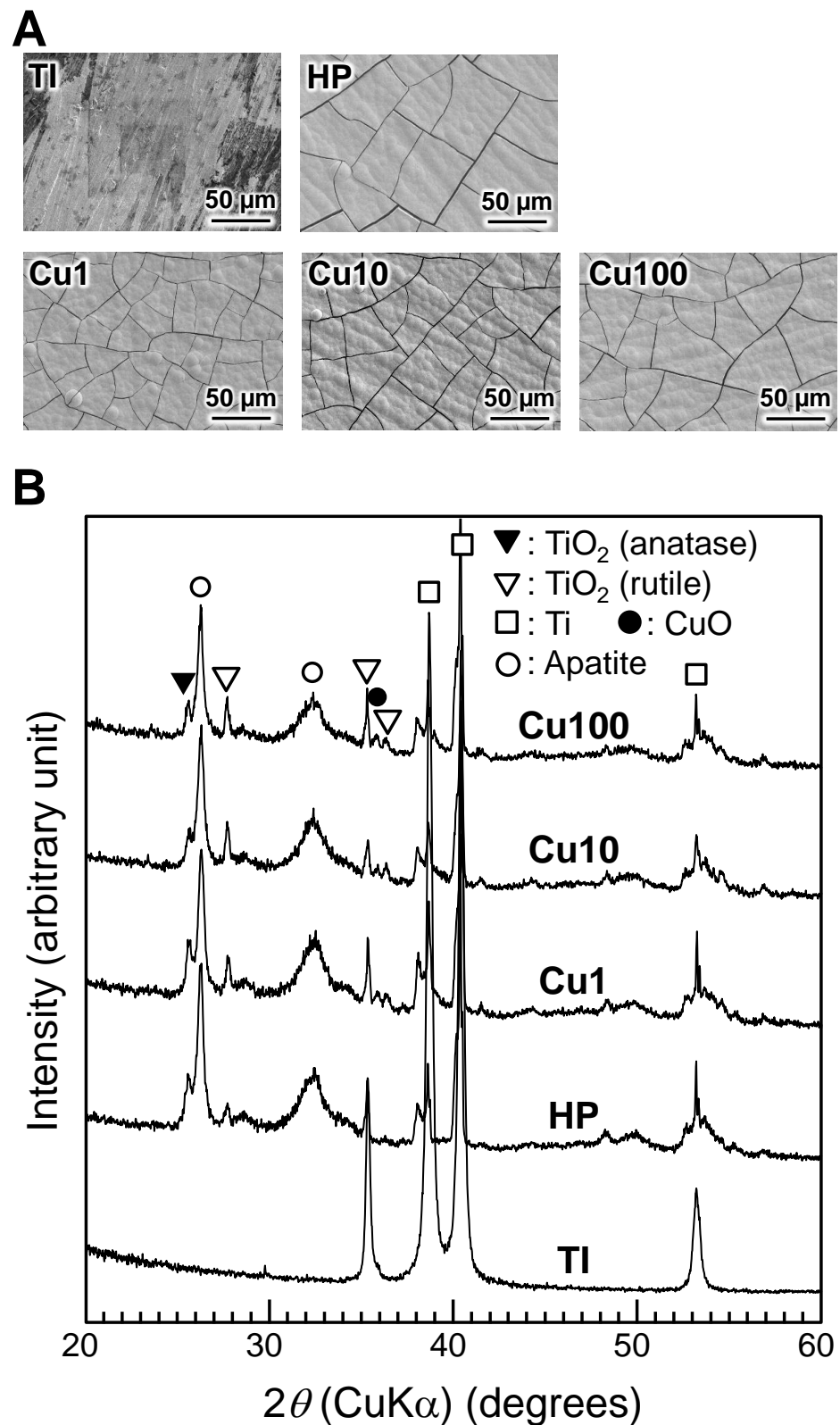


Figure 5. SEM photographs (A) and XRD patterns (B) of samples after 7 days of incubation in SBF. SEM: scanning electron microscope, Ti: sample with no treatment, HP: sample with H_2O_2 treatment, Cu1: sample with H_2O_2 , 1 mM $\text{Cu}(\text{OAc})_2$, and heat treatment, Cu10: sample with H_2O_2 , 10 mM $\text{Cu}(\text{OAc})_2$, and heat treatment, Cu100: sample with H_2O_2 , 100 mM $\text{Cu}(\text{OAc})_2$, and heat treatment, SBF: simulated body fluid.

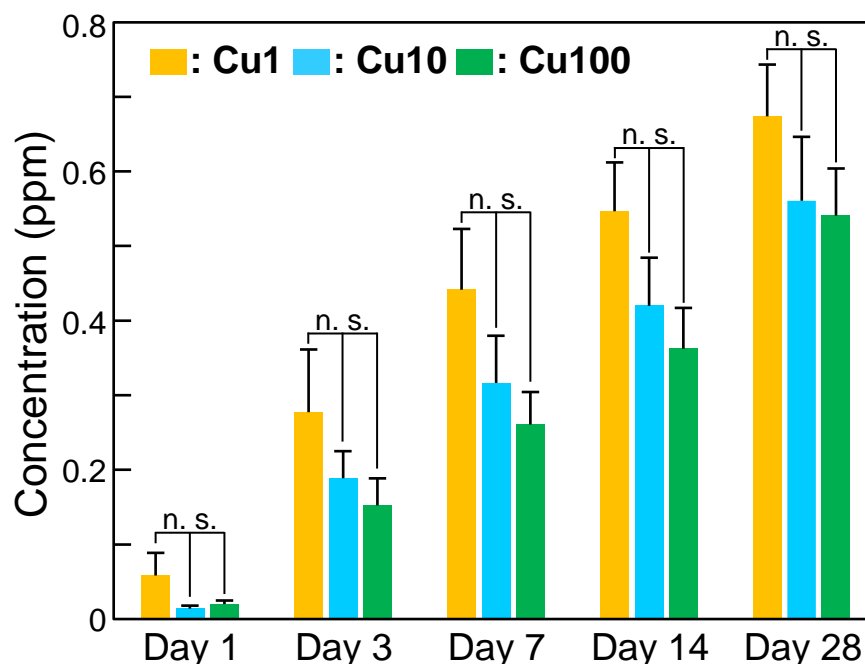


Figure 6. Concentration of Cu eluted from samples into PBS when immersed in PBS for periods of up to 28 days. Values are presented as arithmetic mean \pm SD ($n = 3$). n.s. $p \geq 0.01$ (one-way analysis of variance followed by multiple-hypothesis tests (Tukey’s honestly significant difference tests)). Cu1: sample with H₂O₂, 1 mM Cu(OAc)₂, and heat treatment, Cu10: sample with H₂O₂, 10 mM Cu(OAc)₂, and heat treatment, Cu100: sample with H₂O₂, 100 mM Cu(OAc)₂, and heat treatment, PBS: phosphate-buffered saline, n.s.: not significant.

The ESR spectra of the Cu1, Cu10, and Cu100 samples, with or without visible-light irradiation, exhibited two classes of ESR signals (Figure 8). The first showed hyperfine coupling constants of $a_N = 1.49$ and $a_H = 1.49$ mT and was assigned to DMPO-OH, a spin adduct of DMPO and \cdot OH; the second was an unknown signal. Notably, the intensity of the DMPO-OH peaks was increased by irradiation with visible light. The concentration of hydroxyl radicals (\cdot OH) generated from the samples was elevated by irradiation with visible light, and the \cdot OH concentrations were nominally higher in the Cu1, Cu10, and Cu100 samples compared to the TI and HP samples (Table 3).

Table 3. Concentrations of hydroxyl radical (\cdot OH) generated by samples with and without visible-light irradiation. TI: sample with no treatment, HP: sample with H₂O₂ treatment, Cu1: sample with H₂O₂, 1 mM Cu(OAc)₂, and heat treatment, Cu10: sample with H₂O₂, 10 mM Cu(OAc)₂, and heat treatment, Cu100: sample with H₂O₂, 100 mM Cu(OAc)₂, and heat treatment.

Sample	\cdot OH Concentration (μ M)	
	Without Visible-Light Irradiation	With Visible-Light Irradiation
TI	0.09	0.19
HP	0.21	0.51
Cu1	1.08	3.03
Cu10	1.44	3.23
Cu100	1.50	4.36

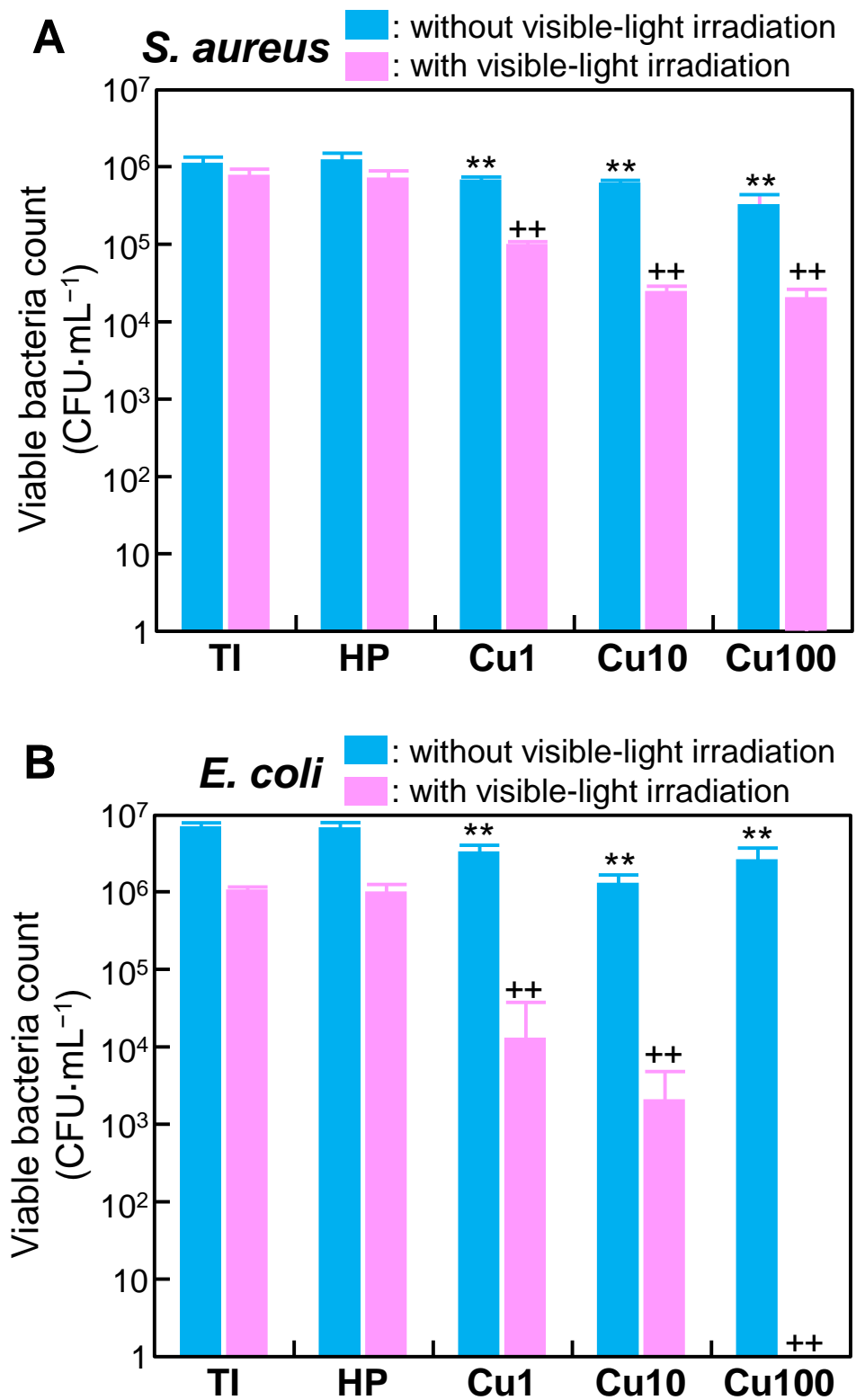


Figure 7. Viable counts of *S. aureus* (A) and *E. coli* (B) in samples without and with visible-light irradiation. Values are presented as arithmetic mean \pm SD ($n = 4$). ** $p < 0.01$ vs. TI without visible-light irradiation, ++ $p < 0.01$ vs. TI with visible-light irradiation (one-way analysis of variance followed by multiple-hypothesis tests (Tukey’s honestly significant difference tests)). CFU: colony-forming unit, TI: sample with no treatment, HP: sample with H₂O₂ treatment, Cu1: sample with H₂O₂, 1 mM Cu(OAc)₂, and heat treatment, Cu10: sample with H₂O₂, 10 mM Cu(Oac)₂, and heat treatment, Cu100: sample with H₂O₂, 100 mM Cu(OAc)₂, and heat treatment.

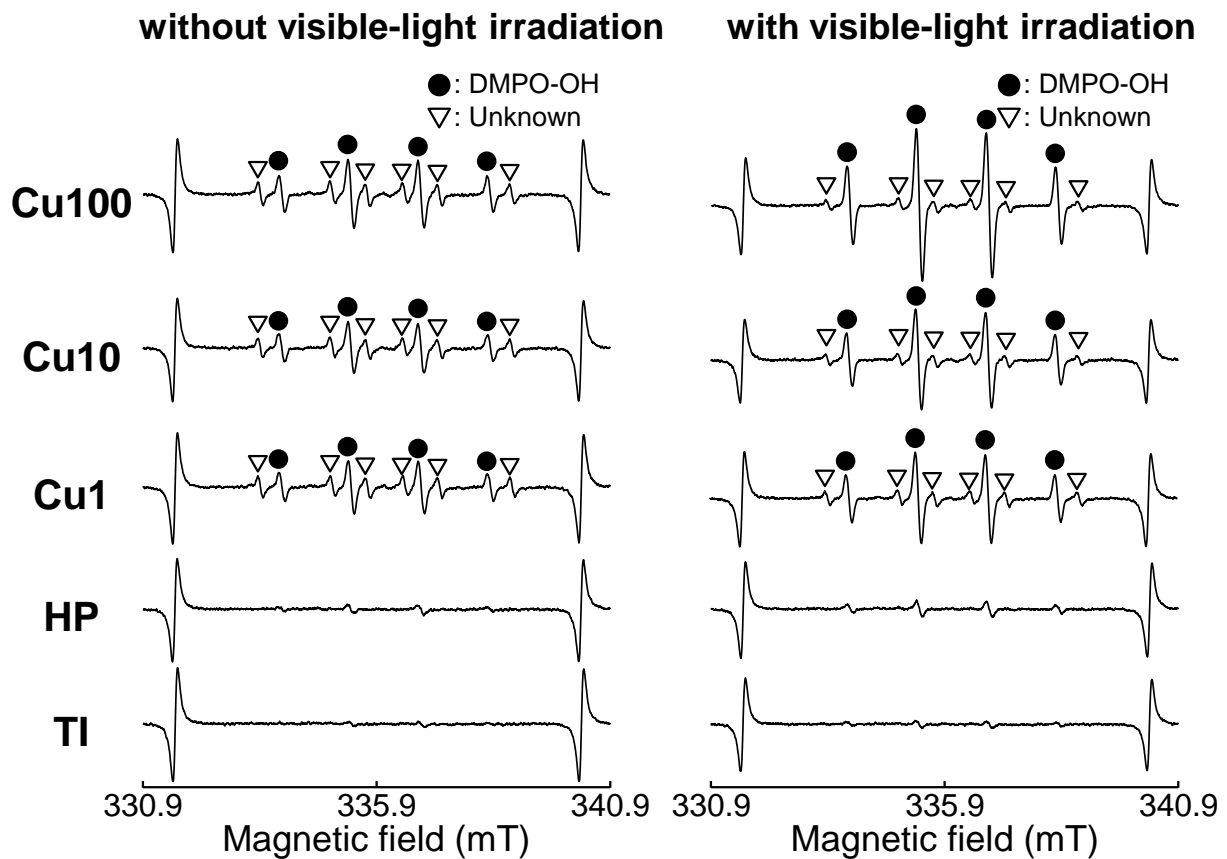
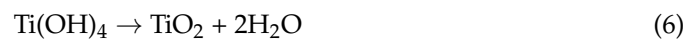
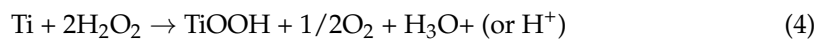


Figure 8. ESR spectra of samples without and with visible-light irradiation. ESR: electron spin resonance, DMPO: 5,5-dimethyl-1-pyrroline-*N*-oxide, TI: sample with no treatment, HP: sample with H₂O₂ treatment, Cu1: sample with H₂O₂, 1 mM Cu(OAc)₂, and heat treatment, Cu10: sample with H₂O₂, 10 mM Cu(OAc)₂, and heat treatment, Cu100: sample with H₂O₂, 100 mM Cu(OAc)₂, and heat treatment.

4. Discussion

Following sequential exposure to H₂O₂, Cu(OAc)₂, and heat (the procedure described in the present work), the surface of the HP sample exhibited a fine network structure consisting of anatase- and rutile-type TiO₂ (Figures 2 and 3A). H₂O₂ has been reported to react with Ti to form TiO₂ on Ti as follows [38].



The TiO₂ fine network structure formed by immersion in H₂O₂ solution remained even after immersion in 100 mM Cu(OAc)₂ solution, indicating that the undesired dissolution of the TiO₂ layer seen upon exposure to strongly acidic Cu solutions was avoided by using a weakly acidic Cu(OAc)₂ solution for Cu doping of the TiO₂. We attribute the observed increase in the intensity ratio of the TiO₂ XRD peaks (ratio of rutile-type to anatase-type) in the Cu1, Cu10, and Cu100 samples (Figure 2) to the enhancement of anatase-to-rutile transformation by Cu doping of the TiO₂ [47–51].

Figures 2–4 and Table 2 indicated that the small particles formed on the Cu1, Cu10, and Cu100 samples are composed primarily of CuO. There are concerns about the stability and durability of small CuO particles [52], but we believe that the small CuO particles are stable and chemically durable, given that the concentration of Cu released from samples

was less than 0.8 ppm, even after soaking in PBS for 28 days (Figure 6), and that the color of samples remained black even after the soaking in PBS. Additionally, the data in Table 2 indicated that the Cu concentration on the sample surface does not increase linearly with the Cu(OAc)₂ concentration, instead showing saturation at about 16 atomic%. In contrast, in our previous study on Ti subjected to NaOH-Cu(NO₃)₂-heat treatments [27], the Cu concentration on the sample surface peaked at approximately 12 atomic%. Although the mechanistic basis for this difference is unknown, the H₂O₂-Cu(OAc)₂-heat treatment proposed in the present work permits the doping of nominally greater levels of Cu onto the sample surface than does the previous NaOH-Cu(NO₃)₂-heat treatments.

All samples other than the TI sample accumulated a dense and uniform surface apatite layer during 7 days of incubation in SBF (Figure 4). Previous work [33] has shown that the anatase- and rutile-type TiO₂ on these sample surfaces (Figure 2) is responsible for the apatite formation during immersion in SBF. The apatite-forming ability of the Cu1, Cu10, and Cu100 samples appeared to be much higher than that seen previously in samples prepared by NaOH-Cu(NO₃)₂-heat treatments [28]. Therefore, the technique described here succeeded in forming Cu-doped TiO₂ with increased apatite-forming ability on Ti. Many factors affect the apatite-forming ability of TiO₂, including the acidity and basicity of Ti-OH groups [53–55], and the crystalline phase [33] and porosity [56] of TiO₂. In addition, the apatite-forming ability of metal-doped TiO₂ on Ti is affected by the chemical state of the doped metal [27]. To gain insight for the preparation of samples with higher apatite-forming ability, it is necessary to identify the factor(s) responsible for the higher apatite-forming ability of the present samples (compared to that of the previous samples). However, we are not able to define the relevant factor(s), given the many differences between the processes used in the present and previous work. Further study will be needed to identify the factor(s) responsible for the higher apatite-forming ability of the present samples. For clinical applications, samples prepared as in the present paper will need to be evaluated *in vivo* for their bone-binding ability. We conjecture that samples prepared as described here will form an apatite layer on their surface even *in vivo*, and that this apatite layer will facilitate direct bonding to living bone [42].

The Cu1, Cu10, and Cu100 samples also showed antibacterial activity against *S. aureus* and *E. coli*, even in the absence of visible-light irradiation (Figure 7). This activity may reflect the combined effects of copper ions released from the sample (Figure 6), contact between bacteria and small CuO particles present on the sample surface [57], and the small amount of ·OH generated from the samples (Table 3). The antibacterial activity of these samples was remarkably enhanced by visible-light irradiation. The generation of ·OH from these samples (Figure 8 and Table 3) may be responsible for the enhanced antibacterial activity of these samples following irradiation with visible light. Notably, the improvement in the antibacterial activity following visible-light irradiation appeared to be more pronounced against *E. coli* than against *S. aureus* (Figure 7B). This distinction may reflect the fact that the peptidoglycan layer in *E. coli*, a Gram-negative bacterium, is thinner than that in *S. aureus*, a Gram-positive bacterium [58,59]. Given that ROS, including ·OH, can induce chronic inflammation, future *in vivo* studies will be needed to investigate any inflammatory responses induced by ROS generated by the samples. However, we conjecture that the inflammatory response(s) induced by ROS generated by the samples will be limited, since the concentration of ·OH was low, and increased only when the sample was irradiated with visible light (Table 3). The antibacterial activity of the samples against other bacteria that cause peri-implantitis, such as *Porphyromonas gingivalis*, should also be investigated in future studies.

In the ESR assessment, DMPO-OH peaks were observed for the Cu1, Cu10, and Cu100 samples, even in the absence of visible-light irradiation (Figure 8). This observation indicated that these samples generate ·OH even in the dark (Table 3). We hypothesize that ·OH is generated when CuO particles present on the sample surface react with the reagent or water used in this experiment [60,61]. The unknown peaks in the ESR spectrum of the sample may be attributable to carbon-centered radicals, such as methyl radicals [62].

These carbon-centered radicals may originate from carbon in reagents decomposed by CuO particles present on the sample surface.

To the eye, the Cu1, Cu10, and Cu100 samples appeared black in color (inset photographs in Figure 3A). This black coloration presumably is attributable to the visible light absorption of the CuO [31,63–68] formed on these samples by heat treatment. For CuO-doped TiO₂, it has been reported that CuO doping extends the tailing of the absorption edge toward the visible region, resulting in band-gap narrowing [64–66]. In addition, the precipitation of fine particles of CuO on the TiO₂ surface (Figure 2) suggests that the visible-light-responsive photocatalytic effect may have been induced by interfacial charge transfer of electrons from TiO₂ to CuO [31,67,68]. Although no clear UV-visible spectrum (which would indicate narrowing of the band gap) was obtained for these samples, we speculate that the Cu-doped TiO₂ formed on Ti by this method exhibits visible-light-responsive photocatalytic activity due to the interface charge transfer between CuO and TiO₂; this activity would result in the observed enhancement of antibacterial activity by visible-light irradiation (Figure 7). Additionally, as shown in Figure 2, CuO small particles formed sparsely on Ti substrate, making it difficult to obtain clear UV-visible spectra of the CuO small particles themselves.

In the present study, we found that H₂O₂-Cu(OAc)₂-heat treatments induced the layering of TiO₂ with CuO fine particles; we further demonstrated that the TiO₂ layer showed apatite-forming ability during incubation in SBF and visible-light-enhanced antibacterial activity. The novelty of our work is that we have succeeded in preparing titanium substrates with CuO-supported TiO₂ surfaces; these substrates exhibited excellent apatite-forming ability and visible-light-enhanced antibacterial activity against both *E. coli* and *S. aureus*. Previous work has shown that apatite-coated TiO₂ powders show antibacterial activity against *E. coli* and *S. aureus* when irradiated with black light or visible light [69], and that TiO₂ layers formed on Ti substrates by Au-sputtering and thermal oxidation show antibacterial activity against *E. coli* when irradiated with visible light [70]. However, to the best of our knowledge, surface-modified titanium substrates with similar functions have not been reported to date. Future investigations will be needed to evaluate the toxicity and bone-bonding ability of samples prepared as described here. Nonetheless, we hypothesize that dental implants with Cu-doped TiO₂ on the abutments may decrease the risk of peri-implantitis when treated in the dental clinic by regular or on-demand irradiation with visible light. Furthermore, if employed for devices that are partially exposed outside the body (such as external fixators), materials with such surfaces are expected to exhibit antibacterial properties when exposed to visible light.

5. Conclusions

A network structure of anatase- and rutile-type TiO₂ with CuO fine particles was generated when Ti was subjected to H₂O₂-Cu(OAc)₂-heat treatments. Such surface-treated Ti accumulated a dense and uniform surface layer of apatite when incubated for 7 days in SBF, indicating enhanced apatite-forming ability compared to that previously reported for Ti subjected to NaOH-Cu(NO₃)₂-heat treatments. Furthermore, samples prepared as described here showed enhanced antibacterial activity against *E. coli* and *S. aureus* when subjected to visible-light irradiation. The increased antibacterial activity of these samples under visible-light irradiation may be attributable to the generation of ·OH by the samples. Together, these results suggest that Ti implants with reduced risk of peri-implantitis following on-demand visible-light irradiation can be obtained by the H₂O₂-Cu(OAc)₂-heat treatments described here.

Author Contributions: Conceptualization, M.K.; methodology, P.-C.S., M.S., T.Y. and T.M.; validation, P.-C.S., M.S., T.Y., T.M. and M.S.; formal analysis, P.-C.S., M.S., T.Y. and T.M.; investigation, P.-C.S., M.S. and T.M.; data curation, P.-C.S., M.S., T.Y. and T.M.; writing—original draft preparation, P.-C.S. and M.K.; writing—review and editing, P.-C.S., M.S., T.Y., T.M. and M.K.; supervision, M.K.; project administration, M.K.; funding acquisition, M.K. All authors have read and agreed to the published version of the manuscript.

Funding: This research was funded by the Japan Society for the Promotion of Science (JSPS) KAKENHI Grant No.: JP16H03177; the Kazuchika Okura Memorial Foundation; and a grant from the Ministry of Education, Culture, Sports, Science and Technology, Japan (MEXT) administered via the Institute of Biomaterials and Bioengineering, Tokyo Medical and Dental University (Project “Design and Engineering by Joint Inverse Innovation for Materials Architecture (DEJI²MA)”).

Data Availability Statement: The raw data supporting the conclusions of this article will be made available by the authors on request.

Conflicts of Interest: The authors declare no conflicts of interest.

References

- Mombelli, A.; Lang, P. The diagnosis and treatment of peri-implantitis. *Periodontology 2000* **1998**, *17*, 63–76. [[CrossRef](#)] [[PubMed](#)]
- Brägger, U.; Aeschlimann, S.; Bürgin, W.; Hämmerle, C.H.; Lang, N.P. Biological and technical complications and failures with fixed partial dentures (FPD) on implants and teeth after four to five years of function. *Clin. Oral Implant. Res.* **2001**, *12*, 26–34. [[CrossRef](#)] [[PubMed](#)]
- Gruica, B.; Wang, H.Y.; Lang, N.P.; Buser, D. Impact of IL-1 genotype and smoking status on the prognosis of osseointegrated implants. *Clin. Oral Implants Res.* **2004**, *15*, 393–400. [[CrossRef](#)] [[PubMed](#)]
- Fransson, C.; Lekholm, U.; Jemt, T.; Berglundh, T. Prevalence of subjects with progressive bone loss at implants. *Clin. Oral Implant. Res.* **2005**, *16*, 440–446. [[CrossRef](#)] [[PubMed](#)]
- Roos-Jansåker, A.M.; Lindahl, C.; Renvert, H.; Renvert, S. Nine-to fourteen-year follow-up of implant treatment, Part I: Implant loss and associations to various factors. *J. Clin. Periodontol.* **2006**, *33*, 283–289. [[CrossRef](#)] [[PubMed](#)]
- Dvorak, G.; Arnhart, C.; Heuberger, S.; Christian, D.; Huber, C.D.; Watzek, G.; Gruber, R. Peri-implantitis and late implant failures in postmenopausal women: A cross-sectional study. *J. Clin. Periodontol.* **2011**, *38*, 950–955. [[CrossRef](#)] [[PubMed](#)]
- Lee, J.C.Y.; Mattheos, N.; Nixon, K.C.; Ivanovski, S. Residual periodontal pockets are a risk indicator for peri-implantitis in patients treated for periodontitis. *Clin. Oral Implant. Res.* **2012**, *23*, 325–333.
- Renvert, S.; Lessem, J.; Dahlén, G.; Renvert, H.; Lindahl, C. Mechanical and repeated antimicrobial therapy using a local drug delivery system in the treatment of peri-implantitis: A randomized clinical trial. *J. Periodontol.* **2008**, *79*, 836–844. [[CrossRef](#)] [[PubMed](#)]
- Bassetti, M.; Schär, D.; Wicki, B.; Eick, S.; Ramseier, C.A.; Arweiler, N.B.; Sculean, A.; Salvi, G.E. Anti-infective therapy of peri-implantitis with adjunctive local drug delivery or photodynamic therapy: 12-month outcomes of a randomized controlled clinical trial. *Clin. Oral Implant. Res.* **2014**, *25*, 279–287. [[CrossRef](#)]
- Dadgostar, P. Antimicrobial resistance: Implications and costs. *Infect. Drug Resist.* **2019**, *12*, 3903–3910. [[CrossRef](#)]
- Chen, J.Y.; Cheng, F.; Luo, D.W.; Huang, J.F.; Ouyang, J.; Nezamzadeh-Ejehieh, A.; Khan, M.S.; Liu, J.Q.; Peng, Y.Q. Recent advances in Ti-based MOFs in biomedical applications. *Dalton Trans.* **2022**, *51*, 14817–14832. [[CrossRef](#)] [[PubMed](#)]
- Gu, B.; Cai, J.; Peng, G.; Zhou, H.; Zhang, W.; Deyuan Zhang, D.; Gong, D. Metal organic framework-loaded biohybrid magnetic microrobots for enhanced antibacterial treatment. *Colloids Surf. A* **2024**, *685*, 133295. [[CrossRef](#)]
- Veerapandian, M.; Yun, K. Functionalization of biomolecules on nanoparticles: Specialized for antibacterial applications. *Appl. Microbiol. Biotechnol.* **2011**, *90*, 1655–1667. [[CrossRef](#)]
- Geng, Z.; Cao, Z.; Liu, J. Recent advances in targeted antibacterial therapy basing on nanomaterials. *Exploration* **2023**, *3*, 20210117. [[CrossRef](#)] [[PubMed](#)]
- Ivanova, E.P.; Hasan, J.; Webb, H.K.; Gervinskis, G.; Juodkakis, S.; Truong, V.K.; Wu, A.H.F.; Lamb, R.N.; Baulin, V.A.; Watson, G.S.; et al. Bactericidal activity of black silicon. *Nat. Commun.* **2013**, *4*, 2838. [[CrossRef](#)] [[PubMed](#)]
- Tarannum, T.; Ahmed, S. Recent development in antiviral surfaces: Impact of topography and environmental conditions. *Helyon* **2023**, *9*, e16698. [[CrossRef](#)] [[PubMed](#)]
- Das, K.; Bose, S.; Bandyopadhyay, A.; Karandikar, B.; Gibbins, B.L. Surface coatings for improvement of bone cell materials and antimicrobial activities of Ti implants. *J. Biomed. Mater. Res. B Appl. Biomater.* **2008**, *87*, 455–460. [[CrossRef](#)] [[PubMed](#)]
- Shimazaki, T.; Miyamoto, H.; Ando, Y.; Noda, I.; Yonekura, Y.; Kawano, S.; Miyazaki, M.; Mawatari, M.; Hotokebuchi, T. In vivo antibacterial and silver-releasing properties of novel thermal sprayed silver-containing hydroxyapatite coating. *J. Biomed. Mater. Res. B Appl. Biomater.* **2010**, *92*, 386–389. [[CrossRef](#)] [[PubMed](#)]
- Shirai, T.; Shimizu, T.; Ohtani, K.; Zen, Y.; Takaya, M.; Tsuchiya, H. Antibacterial iodine-supported titanium implants. *Acta Biomater.* **2011**, *7*, 1928–1933. [[CrossRef](#)]
- Kizuki, T.; Matsushita, T.; Kokubo, T. Antibacterial and bioactive calcium titanate layers formed on Ti metal and its alloys. *J. Mater. Sci. Mater. Med.* **2014**, *25*, 1737–1746. [[CrossRef](#)]
- Shimabukuro, M.; Tsutsumi, Y.; Yamada, R.; Ashida, M.; Chen, P.; Doi, H.; Nozaki, K.; Nagai, A.; Hanawa, T. Investigation of realizing both antibacterial property and osteogenic cell compatibility on titanium surface by simple electrochemical treatment. *ACS Biomater. Sci. Eng.* **2019**, *5*, 5623–5630. [[CrossRef](#)]
- Shimabukuro, M.; Tsutsumi, Y.; Nozaki, K.; Chen, P.; Yamada, R.; Ashida, M.; Doi, H.; Nagai, A.; Hanawa, T. Investigation of antibacterial effect of copper introduced titanium surface by electrochemical treatment against facultative anaerobic bacteria. *Dent. Mater. J.* **2020**, *39*, 639–647. [[CrossRef](#)] [[PubMed](#)]

23. Shimabukuro, M.; Manaka, T.; Tsutsumi, Y.; Nozaki, K.; Chen, P.; Ashida, M.; Nagai, A.; Hanawa, T. Corrosion behavior and bacterial viability on different surface states of copper. *Mater. Trans.* **2020**, *61*, 1143–1148. [[CrossRef](#)]
24. Shimabukuro, M. Antibacterial property and biocompatibility of silver, copper, and zinc in titanium dioxide layers incorporated by one-step micro-arc oxidation: A review. *Antibiotics* **2020**, *9*, 716. [[CrossRef](#)]
25. Aoki, S.; Shimabukuro, M.; Kishida, R.; Kyuno, K.; Noda, K.; Yokoi, T.; Kawashita, M. Electrochemical deposition of copper on bioactive porous titanium dioxide layer: Antibacterial and pro-osteogenic activities. *ACS Appl. Bio Mater.* **2023**, *6*, 5759–5767. [[CrossRef](#)] [[PubMed](#)]
26. Morimoto, T.; Hirata, H.; Eto, S.; Hashimoto, A.; Kii, S.; Kobayashi, T.; Tsukamoto, M.; Yoshihara, T.; Toda, Y.; Mawatari, M. Development of silver-containing hydroxyapatite-coated antimicrobial implants for orthopaedic and spinal surgery. *Medicina* **2022**, *58*, 519. [[CrossRef](#)]
27. Kawashita, M.; Iwabuchi, Y.; Suzuki, K.; Furuya, M.; Yokota, K.K.; Kanetaka, H. Surface structure and in vitro apatite-forming ability of titanium doped with various metals. *Colloids Surf. A* **2018**, *555*, 558–564. [[CrossRef](#)]
28. Suzuki, K.; Yokoi, T.; Iwatsu, M.; Mokudai, T.; Kanetaka, H.; Kawashita, M. Antibacterial properties of Cu-doped TiO₂ prepared by chemical and heat treatment of Ti metal. *J. Asian Ceram. Soc.* **2021**, *9*, 1448–1456. [[CrossRef](#)]
29. Fujibayashi, S.; Nakamura, T.; Nishiguchi, S.; Tamura, J.; Uchida, M.; Kim, H.M.; Kokubo, T. Bioactive titanium: Effect of sodium removal on the bone-bonding ability of bioactive titanium prepared by alkali and heat treatment. *J. Biomed. Mater. Res.* **2001**, *56*, 562–570. [[CrossRef](#)]
30. Yadav, H.M.; Otari, S.V.; Koli, V.B.; Mali, S.S.; Hong, C.K.; Pawar, S.H.; Delekar, S.D. Preparation and characterization of copper-doped anatase TiO₂ nanoparticles with visible light photocatalytic antibacterial activity. *J. Photochem. Photobiol. A* **2014**, *280*, 32–38. [[CrossRef](#)]
31. Liu, M.; Sunada, K.; Hashimoto, K.; Miyauchi, M. Visible-light sensitive Cu(II)-TiO₂ with sustained anti-viral activity for efficient indoor environmental remediation. *J. Mater. Chem. A* **2015**, *3*, 17312–17319. [[CrossRef](#)]
32. Mathew, S.; Ganguly, P.; Rhatigan, S.; Kumaravel, V.; Byrne, C.; Hinder, S.J.; Bartlett, J.; Nolan, M.; Pillai, S.C. Cu-doped TiO₂: Visible light assisted photocatalytic antimicrobial activity. *Appl. Sci.* **2018**, *8*, 2067. [[CrossRef](#)]
33. Uchida, M.; Kim, H.M.; Kokubo, T.; Fujibayashi, S.; Nakamura, T. Structural dependence of apatite formation on titania gels in a simulated body fluid. *J. Biomed. Mater. Res. Part A* **2003**, *64*, 164–170. [[CrossRef](#)] [[PubMed](#)]
34. Ohtsuki, C.; Iida, H.; Hayakawa, S.; Osaka, A. Bioactivity of titanium treated with hydrogen peroxide solutions containing metal chlorides. *J. Biomed. Mater. Res.* **1997**, *35*, 39–47. [[CrossRef](#)]
35. Kaneko, S.; Tsuru, K.; Hayakawa, S.; Takemoto, S.; Ohtsuki, C.; Ozaki, T.; Inoue, H.; Osaka, A. In vivo evaluation of bone-bonding of titanium metal chemically treated with a hydrogen peroxide solution containing tantalum chloride. *Biomaterials* **2001**, *22*, 875–881. [[CrossRef](#)] [[PubMed](#)]
36. Wu, J.M.; Hayakawa, S.; Tsuru, K.; Osaka, A. Crystallization of anatase from amorphous titania in hot water and in vitro biomineralization. *J. Ceram. Soc. Jpn.* **2002**, *110*, 78–80. [[CrossRef](#)]
37. Wang, X.X.; Hayakawa, S.; Tsuru, K.; Osaka, A. Bioactive titania gel layers formed by chemical treatment of Ti substrate with a H₂O₂/HCl solution. *Biomaterials* **2002**, *23*, 1353–1357. [[CrossRef](#)] [[PubMed](#)]
38. Osaka, A.; Tsuru, K.; Hayakawa, S. Titania derived from combined chemical and thermal treatments of titanium: In vitro apatite forming ability. *Phosphorus Res. Bull.* **2004**, *17*, 130–141. [[CrossRef](#)] [[PubMed](#)]
39. Suzuki, K.; Iwatsu, M.; Mokudai, T.; Furuya, M.; Yokota, K.; Kanetaka, H.; Shimabukuro, M.; Yokoi, T.; Kawashita, M. Visible-light-enhanced antibacterial activity of silver and copper co-doped titania formed on titanium via chemical and thermal treatments. *Molecules* **2023**, *28*, 650. [[CrossRef](#)]
40. Shirley, D.A. High-resolution X-ray photoemission spectrum of the valence bands of gold. *Phys. Rev. B* **1972**, *5*, 4709–4714. [[CrossRef](#)]
41. Biesinger, M.C. Advanced analysis of copper X-ray photoelectron spectra. *Surf. Interf. Anal.* **2017**, *49*, 1325–1334. [[CrossRef](#)]
42. Kokubo, T.; Takadama, H. How useful is SBF in predicting in vivo bone bioactivity? *Biomaterials* **2006**, *27*, 2907–2915. [[CrossRef](#)]
43. ISO 23317:2014; Implants for Surgery—In Vitro Evaluation for Apatite-Forming Ability of Implant Materials. International Organization for Standardization: Geneva, Switzerland, 2014.
44. JIS R 1752:2020; Fine Ceramics (Advanced Ceramics, Advanced Technical Ceramics)—Test Method for Antibacterial Activity of Photocatalytic Materials and Efficacy under Indoor Lighting Environment. Japanese Standards Association: Tokyo, Japan, 2020.
45. Georgiadou, I.; Spanos, N.; Papadopoulou, C.; Matralis, H.; Kordulis, C.; Lycourghiotis, A. Preparation and characterization of various titanias (anatase) used as supports for vanadia-supported catalysts. *Colloids Surf. A* **1995**, *98*, 155–165. [[CrossRef](#)]
46. Shimabukuro, M.; Kobayashi, M.; Kawashita, M. Metallic substrate influences on the osteogenic cell compatibility and antibacterial activity of silver-incorporated porous oxide layers formed by micro-arc oxidation. *ACS Appl. Eng. Mater.* **2023**, *1*, 2288–2294. [[CrossRef](#)]
47. Iida, Y.; Ozaki, S. Grain growth and phase transformation of titanium oxide during calcination. *J. Am. Ceram. Soc.* **1961**, *44*, 120–127. [[CrossRef](#)]
48. Shannon, R.D.; Pask, J.A. Kinetics of the anatase-rutile transformation. *J. Am. Ceram. Soc.* **1965**, *48*, 391–398. [[CrossRef](#)]
49. MacKenzie, K.J.D. Calcination of titania V. Kinetics and mechanism of the anatase-rutile transformation in the presence of additives. *Trans. J. Br. Ceram. Soc.* **1975**, *74*, 77–84.
50. Kim, D.W.; Kim, T.G.; Hong, K.S. Low-firing of CuO-doped anatase. *Mater. Res. Bull.* **1999**, *34*, 771–781. [[CrossRef](#)]

51. Hanaor, D.A.H.; Sorrell, C.C. Review of the anatase to rutile phase transformation. *J. Mater. Sci.* **2011**, *46*, 855–874. [[CrossRef](#)]
52. Sajjad, H.; Sajjad, A.; Haya, R.T.; Khan, M.M.; Zia, M. Copper oxide nanoparticles: In vitro and in vivo toxicity, mechanisms of action and factors influencing their toxicology. *Comp. Biochem. Physiol. C Toxicol. Pharmacol.* **2023**, *271*, 109682. [[CrossRef](#)]
53. Kasuga, T.; Kondo, H.; Nogami, M. Apatite formation on TiO₂ in simulated body fluid. *J. Crystal Growth* **2002**, *235*, 235–240. [[CrossRef](#)]
54. Kokubo, T.; Yamaguchi, S. Novel bioactive materials developed by simulated body fluid evaluation: Surface-modified Ti metal and its alloys. *Acta Biomater.* **2016**, *44*, 16–30. [[CrossRef](#)] [[PubMed](#)]
55. Ferraris, S.; Yamaguchi, S.; Barbani, N.; Cazzola, M.; Cristallini, C.; Miola, M.; Vernè, E.; Spriano, S. Bioactive materials: In vitro investigation of different mechanisms of hydroxyapatite precipitation. *Acta Biomater.* **2020**, *102*, 468–480. [[CrossRef](#)] [[PubMed](#)]
56. Li, Z.; Miyazaki, T.; Kawashita, M. Preparation and in vitro apatite-forming ability of porous and non-porous titania microspheres. *J. Ceram. Soc. Jpn.* **2013**, *121*, 782–787. [[CrossRef](#)]
57. Hans, M.; Erbe, A.; Mathews, S.; Chen, Y.; Solioz, M.; Mücklich, F. Role of copper oxides in contact killing of bacteria. *Langmuir* **2013**, *29*, 16160–16166. [[CrossRef](#)] [[PubMed](#)]
58. Louis, P.; Trüper, H.G.; Galinski, E.A. Survival of *Escherichia coli* during drying and storage in the presence of compatible solutes. *Appl. Microbiol. Biotechnol.* **1994**, *41*, 684–688. [[CrossRef](#)]
59. Sunada, K.; Watanabe, T.; Hashimoto, K. Studies on photokilling of bacteria on TiO₂ thin film. *J. Photochem. Photobiol. A* **2003**, *156*, 227–233. [[CrossRef](#)]
60. Hricovíni, M.; Mazúr, M.; Sîrbu, A.; Palamarciuc, O.; Arion, V.B.; Brezová, V. Copper (II) thiosemicarbazone complexes and their proligands upon UVA irradiation: An EPR and spectrophotometric steady-state study. *Molecules* **2018**, *23*, 721. [[CrossRef](#)] [[PubMed](#)]
61. Zhao, S.; Miao, D.; Zhu, K.; Tao, K.; Wang, C.; Sharma, V.K.; Jia, H. Interaction of benzo [a] pyrene with Cu (II)-montmorillonite: Generation and toxicity of environmentally persistent free radicals and reactive oxygen species. *Environ. Int.* **2019**, *129*, 154–163. [[CrossRef](#)] [[PubMed](#)]
62. Kuppasamy, P.; Zweier, J.L. Characterization of free radical generation by xanthine oxidase: Evidence for hydroxyl radical generation. *J. Biol. Chem.* **1989**, *264*, 9880–9884. [[CrossRef](#)]
63. Colón, G.; Maicu, M.; Hidalgo, M.C.; Navío, J.A. Cu-doped TiO₂ systems with improved photocatalytic activity. *Appl. Catal. B* **2006**, *67*, 41–51. [[CrossRef](#)]
64. Ni, Y.; Zhu, Y.; Ma, X. A simple solution combustion route for the preparation of metal-doped TiO₂ nanoparticles and their photocatalytic degradation properties. *Dalton Trans.* **2011**, *14*, 3689–3694. [[CrossRef](#)] [[PubMed](#)]
65. Ravishankar, T.N.; Vaz, M.d.O.; Teixeira, S.R. The effects of surfactant in the sol-gel synthesis of CuO/TiO₂ nanocomposites on its photocatalytic activities under UV-visible and visible light illuminations. *New J. Chem.* **2020**, *44*, 1888–1904. [[CrossRef](#)]
66. Hernández-Gordillo, A.; Arriaga, S. Mesoporous TiO₂ monoliths impregnated with CdS and CuO nanoparticles for airborne bacteria inactivation under visible light. *Catal. Lett.* **2022**, *152*, 629–640. [[CrossRef](#)] [[PubMed](#)]
67. Irie, H.; Kamiya, K.; Shibamura, T.; Miura, S.; Tryk, D.A.; Yokoyama, T.; Hashimoto, K. Visible light-sensitive Cu(II)-grafted TiO₂ photocatalysts: Activities and X-ray absorption fine structure analyses. *J. Phys. Chem. C* **2009**, *113*, 10761–10766. [[CrossRef](#)]
68. Moniz, S.J.A.; Tang, J. Charge transfer and photocatalytic activity in CuO/TiO₂ nanoparticle heterojunctions synthesised through a rapid, one-pot, microwave solvothermal route. *ChemCatChem* **2015**, *7*, 1659–1667. [[CrossRef](#)]
69. Kangwansupamonkon, W.; Lauruengtana, V.; Surassmo, S.; Ruktanonchai, U. Antibacterial effect of apatite-coated titanium dioxide for textiles applications. *Nanomed. Nanotechnol. Biol. Med.* **2009**, *5*, 240–249. [[CrossRef](#)]
70. Ueda, T.; Koizumi, R.; Ueda, K.; Ito, K.; Ogasawara, K.; Kanetaka, H.; Narushima, T. Antibacterial properties of TiO₂ layers formed by Au-sputtering and thermal oxidation of titanium under visible light. *Mater. Trans.* **2023**, *64*, 155–164. [[CrossRef](#)]

Disclaimer/Publisher's Note: The statements, opinions and data contained in all publications are solely those of the individual author(s) and contributor(s) and not of MDPI and/or the editor(s). MDPI and/or the editor(s) disclaim responsibility for any injury to people or property resulting from any ideas, methods, instructions or products referred to in the content.